Numerical Heat Transfer, Part A, 45: 911–933, 2004

ISSN: 1040-7782 print/1521-0634 online
DOI: 10.1080/10407780490440372

Taylor & Francis
Taylor & Francis Group

NUMERICAL SIMULATION OF TURBULENT FLOW IN SMALL-ANGLE DIFFUSERS AND CONTRACTIONS USING A NEW WALL TREATMENT AND A LINEAR HIGH REYNOLDS k–ε MODEL

Edimilson J. Braga and Marcelo J. S. de Lemos
Departamento de Energia, Instituto Tecnológico de Aeronáutica, São José dos Campos, SP, Brazil.

This work presents numerical prediction for the turbulent flow field confined in a circular duct past a segment of gradually varying cross section. Both expanding and contracting sections are investigated. Equations of boundary-layer type are used and the linear k–ε model, in its high Reynolds form, is applied. A new correlation for treating the grid point closest to the wall is proposed. A marching-forward method is employed for sweeping the computational domain. Computations are first performed for developing and fully developed constant-area ducts in order to assess the reliability of the code. Results are then presented for contractions and diffusers, where comparisons with experimental data for air and water are carried out. Turbulence damping in contractions and its enhancement in diffusers are calculated correctly. Further, for contractions with angles of up to 21°, the use of a parabolic solver shows good agreement with experimental values for the mean and statistical quantities. For diffusers, adverse pressure gradient along the flow limits the quality of the predictions as the angle and length of diffuser increase past 5° and 10 duct radii, respectively.

INTRODUCTION

Passages with gradual contractions and enlargements are found in a number of types of engineering equipment. Turbulent flows within such ducts can be encountered in industrial piping, jetpumps, gas turbines, and air conditioning ducts, for example. Accurate determination of flow mixing and heat transfer rates in such devices contributes to efficiency increase, optimal design parameters, and, ultimately, reduction of the cost–benefit relationship.

Accordingly, the use of simple numerical tools for initial engineering estimates, instead of using memory-demanding, large computational fluid dynamics (CFD) codes, can benefit the overall design process if repetitive calculations are mandatory. If no back flow is in order, marching-forward techniques, implemented along with

Received 14 February 2003; accepted 11 December 2003.
The authors are thankful to CNPq, Brazil, for financial support during the course of this work.
Address correspondence to Marcelo J. S. de Lemos, Departamento de Energia—IEME, Instituto Tecnológico de Aeronáutica—ITA, 12228–900 São José dos Campos, SP, Brazil. E-mail: delemos@mec.ita.br

NOMENCLATURE

c_p	pressure recovery coefficient, Eq. (20)	y	transverse coordinate for boundary layer ($r = y$ for internal flow)
c_μ	constant in Prandtl-Kolmogorov expression	k/U_m^2	nondimensional turbulence kinetic energy
c_1	k–ε model constant	y_N^+	nondimensional wall distance for first grid point, Eq. (12)
c_2	k–ε model constant	α	parameter for radial grid distribution, Eq. (16)
D	duct diameter	β	parameter for axial integration step, Eq. (15)
E	wall law constant	Γ_{eff}^k	effective transport coefficient for k, $(= \mu + \mu_t/\sigma_k)$
f	friction factor	Γ_{eff}^ε	effective transport coefficient for ε, $(= \mu + \mu_t/\sigma_\epsilon)$
f_∞	friction factor for fully developed flow	Γ_{eff}^ϕ	effective transport coefficient for general variable ϕ ($= u, k, \varepsilon$)
f/f_m	friction factor ratio	ε	Dissipation rate of k
k	turbulent kinetic energy per unit mass $(\overline{u_i u_i}/2)$	θ	angle of duct wall with horizontal
m_E''	external surface mass flux in boundary layer	K	von Kármán constant
m_I''	internal surface mass flux in boundary layer	μ	fluid dynamic viscosity
N	number of grid points in transverse direction	μ_{eff}	effective transport coefficient for u $(= \mu + \mu_t)$ Eq. (3)
p	static pressure	μ_t	turbulent momentum transport coefficient $(= \rho c_\mu k^2/\varepsilon)$, Eq. (4)
P	production rate of k $[= \mu_t/\rho\,(\partial u/\partial y)^2]$, Eq. (6)	ρ	fluid density
r	radial coordinate	σ_k	turbulent Prandtl/Schmidt number for k
r_E	external radius of boundary layer	σ_ε	turbulent Prandtl/Schmidt number for ε
r_I	internal radius of boundary layer	τ_w	wall shear stress
R	duct radius	ϕ	general dependent variable ($= u, k, \varepsilon$)
Re	Reynolds number	Ψ	stream function
S_ϕ	source term for ϕ ($= u, k, \varepsilon$)	Ψ_E	value of Ψ at external surface of boundary layer
u	axial velocity	Ψ_{EI}	$\Psi_E - \Psi_I$
u/U_m	nondimensional mean velocity	Ψ_I	value of Ψ at internal surface of boundary layer
U_m	mean velocity		
U^*	friction velocity		
U^+	nondimensional velocity in wall coordinates, Eq. (12).		
v	transverse velocity		
x	axial coordinate		
y'	wall distance $(= R - y)$		

isotropic turbulence models, provide an economical means for conceptual design using cheaper PC-based workstations.

Today, advanced CFD codes such as CFX, FLUENT, ANSYS, and STAR-CD, among many other available fluid solvers, are able to handle structured as well as unstructured grids using a number of different turbulence models. Accordingly, for simulating a complex geometry, the block-structure approach can be applied, in which the flow equations are solved in each block, exchanging boundary information repetitively in order to bring down the residue in each region. In some cases, the overall numerical solution may suffer from long computing times and, on blocks where the flow presents a clear preferential direction, with no recirculating regions, then within that particular region the procedure discussed herein could be applied. Ultimately, in complex flow analyses, one can use different flow models (parabolic or

elliptic) for handling different blocks, contributing to the overall robustness of the entire solution process.

For code validation, the compilation work of Spencer et al. 1995 [1] seems to be the only available experimental data bank for turbulent flow within gradual contractions and diffusers. Therein, experimental data from 11 institutions around the world, taken for flow of air and water in a contraction and in a diffuser, were compared with each other and with computational results using commercial CFD codes. To the best of the authors' knowledge, other than the experiments in [1], most data published on turbulent ducted flows deal with jets undergoing a sudden expansion. When validating flow simulations using simpler parabolic codes, measurements involving abrupt flow expansions can no longer be used for comparison, at least in the near-field region.

Examples of recirculating flow past an abrupt expansion are jets flowing into a stagnant surrounding [2] or within a confining duct [3]. Measurements in two-phase systems [4,5] and computational studies applying large–eddy simulation to coaxial jets are also found in the literature [6]. Yule and Damou [7] presented results for confined coaxial turbulent jets with velocity ratio U_1/U_2 up to 30, U_1 being the central jet velocity. Both streams flowed into a convergent-divergent channel. The report was limited to mean axial velocity and axial turbulent intensity, yet their overall duct length was of a relative short size ($x/D = 4$).

Acknowledging the advantages of "fast" parabolic solvers, Matsumoto and de Lemos [8] presented results for the developing time-averaged and turbulent fields in a coaxial jet along a circular duct of constant area. Later, de Lemos and Milan [9] extended their calculations to flow in long ducts through varying cross sections. De Lemos and Braga [10] further considered coaxial jets with higher and lower annular velocities in diverging and converging ducts of sinusoidal shape. Similar results for ducts with plane walls have also been documented [11]. Experimentally observed turbulence damping in contractions and corresponding enhancement in diffusers, reported in detail by Spencer et al. [1], was correctly simulated by de Lemos and Braga [12]. In that report, direct comparisons with experimental data showed that for contractions up to 21° and for diffusers up to 5°, the model and numerical scheme employed reproduced the basic features of the flow. Beyond those values, as expected, deterioration of the prediction quality was observed, since parabolic equations were considered.

Heat transfer analysis followed with the work of de Lemos and Braga [13], who reported Nusselt numbers and turbulent kinetic energy in planar diffusers and contractions. Therein, flow and heat transfer properties of coaxial jets with higher inner velocity ($U_i > U_e$) and temperature ($T_i > T_e$) were predicted. That work made use of the standard k–ε model, wall log laws for velocity and temperature, and the assumption of constant turbulent Prandtl number. Interesting dissimilarity between heat transport and turbulence was calculated and discussed. While turbulence was damped along accelerating flows (contractions), heat transfer was increased by a fair amount.

The objective of this article is to show that for contractions with angles of up to 21°, the use of a parabolic solver can capture the basic features of the flow if care is taken in the discretization process, if proper grid layout is used, and if an adequate integration step size is employed due to boundary-layer growth along the flow.

For diffusers, adverse pressure gradient along the flow limits the quality of the predictions as the angle and length of diffuser increase past 5° and 10 duct radii, respectively.

MATHEMATICAL MODEL

Geometry

The flow analyzed here consists of a confined stream inside a circular duct of varying cross section. Only situations of gradual area variation are considered here because of the parabolic character of the system of equations comprising the mathematical model. A schematic of the geometry considered is shown in Figure 1*a*. The configuration under study consists of diffusers and contractions of a conical wall. It should be pointed out that in ducts with varying cross section, "recirculating zones" are observed experimentally close to the walls whenever the value of angle θ in an expansion is high. In contractions, the "vena contracta" effect is also observed downstream as an abrupt area reduction. In those cases, as already pointed out, boundary-layer treatment of the flow is no longer valid. This work does not consider cases involving any kind of recirculating zone.

Boundary-Layer Equations for Turbulent Flow

For generality, the equations below are written embracing planar and axisymmetric cases. The equations are also presented in a simplified form, making use of the concept of turbulent viscosity, μ_t. In this concept, the time-averaged Reynolds stresses are taken as proportional to the rate of the deformation tensor. Models that fall into this category are called isotropic turbulence models.

Accordingly, the equations of conservation of mass and x momentum for a two-dimensional, source-free, low-speed, planar/axisymmetric turbulent boundary (mixing) layer can be written as

$$\frac{\partial(r^\eta \rho u)}{\partial x} + \frac{\partial(r^\eta \rho v)}{\partial y} = 0 \tag{1}$$

$$\rho u \frac{\partial u}{\partial x} + \rho v \frac{\partial u}{\partial y} = -\frac{\partial k}{\partial x} + \frac{1}{r^\eta}\frac{\partial}{\partial y}\left(r^\eta \mu_{\text{eff}} \frac{\partial u}{\partial y}\right) \tag{2}$$

In Eqs. (1)–(2) u, v are the velocity components in the axial and transverse directions, respectively, ρ is the fluid density, p is the static pressure, and μ_{eff} is the effective (turbulent + laminar) coefficient of exchange, given as

$$\mu_{\text{eff}} = \mu + \mu_t \tag{3}$$

Also, in Eq. (3), μ is the molecular viscosity. As mentioned before, Eqs. (1)–(2) are written in a compact notation embracing planar ($\eta = 0$) and axisymmetric ($\eta = 1$) cases.

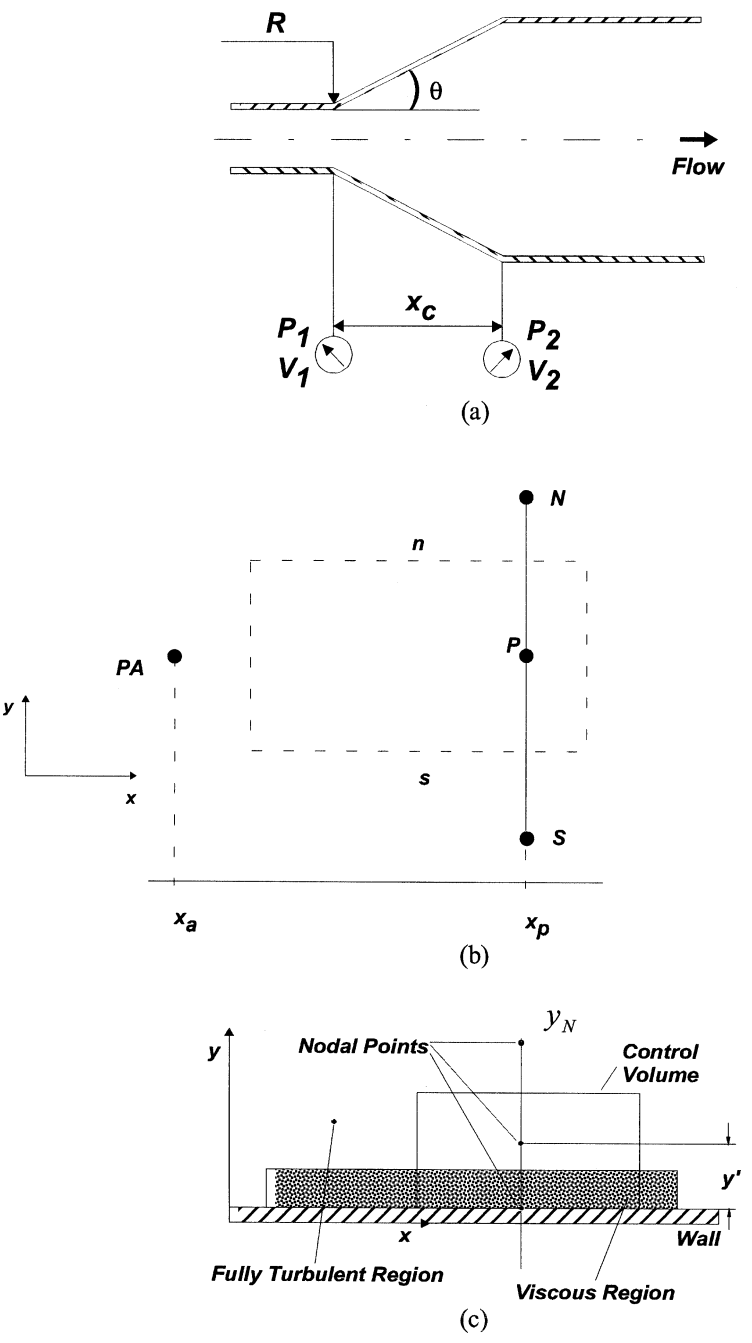

Figure 1. General notation. (*a*) Conical duct: $\theta > 0$, diffuser, $\theta < 0$, contraction, (*b*) Control volume. (*c*) Wall layer model.

The standard k–ε turbulence model [14] has been extensively used in the literature for its characteristics of robustness and numerical stability. Recent extensions of its applicability to a wide variety of flows include the so-called RNG and nonlinear approaches [15]. In fact, the basic advantage of such nonlinear closures over more complex models, e.g., the algebraic stress model (ASM) [16–18], lies in the achieved computational savings (roughly 25–50% less computing time). Basically, the standard k–ε model embodies the early idea of Prandtl/Kolmogorov that, in a turbulent flow, the apparent viscosity μ_t can be considered as proportional to the product of a characteristic velocity scale, V', and a characteristic length scale, L'. In the k–ε model, the characteristic velocity scale is given by $V' = k^{1/2}$, and the characteristic length scale is written as $L' = k^{3/2}/\varepsilon$, implying, for the turbulent viscosity,

$$\mu_t = \rho c_\mu k^2/\varepsilon \tag{4}$$

where c_μ is a constant. Here, only the case involving flow regions of high local Reynolds numbers, or say, regions with Kolmogorov and macroscopic scales adequately separated, is considered [19]. With this, transport equations for k and ε can be written as

$$\begin{aligned} \rho u \frac{\partial k}{\partial x} + \rho v \frac{\partial k}{\partial y} &= \frac{1}{r^\eta} \frac{\partial}{\partial y} \left(r^\eta \Gamma^k_{\text{eff}} \frac{\partial k}{\partial y} \right) + S_k \\ \rho u \frac{\partial \varepsilon}{\partial x} + \rho v \frac{\partial \varepsilon}{\partial y} &= \frac{1}{r^\eta} \frac{\partial}{\partial y} \left(r^\eta \Gamma^\varepsilon_{\text{eff}} \frac{\partial \varepsilon}{\partial y} \right) + S_\varepsilon \end{aligned} \tag{5}$$

In Eq. (5), Γ^k_{eff} and $\Gamma^\varepsilon_{\text{eff}}$ are given by $\Gamma^k_{\text{eff}} = \mu + \mu_1/\sigma_k$ and $\Gamma^\varepsilon_{\text{eff}} = \mu + \mu_t/\sigma_\varepsilon$, where the γ's are the effective coefficients of exchange (laminar + turbulent) and the σ's are turbulent Prandtl/Schmidt numbers for k and ε. The last terms in Eq. (5) are known as "source" terms and are given by $S_k = \rho(P - \varepsilon)$ and $S_c = \rho(\varepsilon/k)(c_1 P - c_2 \varepsilon)$, where $c_1 = 1.47$, $c_2 = 1.92$, and $c_\mu = 0.09$. The production term reads

$$P = \frac{\mu_t}{\rho} \left[\frac{\partial U}{\partial y} \right]^2 \tag{6}$$

NUMERICAL METHOD

The numerical solution of Eqs. (1), (2), and (5) follows the boundary-layer methodology fully explained by Patankar and Spalding [20, 21], where more details can be found. Essentially, a nondimensional coordinate system based on the stream function is used to lay down grid points along the radial coordinate. An example of the control volume for parabolic flows is illustrated in Figure 1*b*. Inlet flow is given a uniform distribution and the values of k and ε at the entrance were assumed as

$$k_{\text{in}} = \mathbf{C} U_m^2 \tag{7}$$

and

$$\varepsilon_{\text{in}} = \frac{k_{\text{in}}^{3/2}}{Ky'} \tag{8}$$

where **C** is a constant, U_m is the overall mean velocity, K is the von Kármán constant (K = 0.4), and y' is the distance to the wall. The constant **C** in Eq. (7) depends on the level of turbulence intensity that is assumed at the inlet. If the turbulence intensity is defined as

$$\text{Tu} = \frac{\sqrt{3\overline{(u_i')^2}}}{U_m} \tag{9}$$

where u_i' is the fluctuating component in the axial direction and the average velocity U_m is the reference velocity, an inlet value for k can be given for isotropic turbulence as

$$k_{\text{in}} = \frac{3}{2}\overline{(u_i')^2} = \left(\frac{1}{2}\ \text{Tu}^2\right) U_m^2 \tag{10}$$

For the centerline ($y = 0$), the symmetry condition is implemented for all dependent variables $\phi = u, k, \varepsilon$, as

$$\left.\frac{\partial \phi}{\partial y}\right|_{y=0} = 0$$

Wall treatment. The mathematical model seen above is not valid inside the layers very close to the wall, where viscous effects are predominant. Velocity at the grid point closest to the wall is handled by the usual wall function approach described by Launder and Spalding [19, 22]. Even though it is recognized that standard wall function treatment may be influenced by variations in the pressure gradient due to flow in enlarging and contracting sections, its use is adopted here for the sake of simplicity. The notation below refers to Figure 1*c* where the location of the first grid point close to the wall, N is identified. the wall function gives for the wall shear stress at node N,

$$\tau_w = \left(U_N \rho c_\mu^{1/4} k_N^{1/2}\right) \Bigg/ \frac{1}{\text{K}} \ln\left[E y_N \frac{\rho (c_\mu^{1/2} k_N)^{1/2}}{\mu}\right] \tag{11}$$

where E a constant. In Eq. (11) the subscript N identifies the grid point closest to the wall. In that region, the use of the wall function, characterized by the expressions

$$U_N^+ = \frac{1}{\text{K}} \ln\left(y_N^+ E\right) \qquad U_N^+ = \frac{u_N}{U^*} \qquad y_N^+ = \frac{\mu y_N U^*}{\rho} \qquad U^* = \sqrt{\frac{\tau_w}{\rho}} \tag{12}$$

and associated with the assumption of "local equilibrium" for turbulence ($P = \varepsilon$), gives for point N,

$$k_N = \frac{\tau_w}{(\rho c_\mu)^{1/2}} \qquad \varepsilon_N = \frac{k_N^{3/2}}{\mathrm{K} y'_N} \tag{13}$$

Rewriting Eq. (11) in the form $\tau_w = \lambda\mu(\partial U/\partial y)$ gives

$$\lambda = \begin{cases} 1 & \text{for laminar flow} \\ \dfrac{K y_N \left[\frac{\rho(c_\mu^{1/2} k_N)^{1/2}}{\mu}\right]}{\ln\left\{E y_N \left[\frac{\rho(c_\mu^{1/2} k_N)^{1/2}}{\mu}\right]\right\}} & \text{for turbulent flow} \end{cases} \tag{14}$$

Numerical Algorithm And Computational Details

Treatment of unknown pressure gradient. To obtain a velocity profile at the downstream position x_p, it is necessary to know the pressure gradient dp/dx. For internal flows, however, the pressure gradient is not known a priori and must be determined during the calculation. Determination of the unknown pressure gradient is handled here as in Patankar, 1988 [21]. With these restrictions applied, the axial momentum equation can be solved with well-known marching-forward numerical techniques for computation of parabolic and partially parabolic flows.

Solution of system of algebraic equations. For the solution of the algebraic system of equations is adopted here the well-known method known as the tri-diagonal matrix algorithm (TDMA) also referred to as the Thomas algorithm. This method takes advantage of the high sparcity degree presented by the coefficient matrix, having only three diagonals and being easily inverted.

Numerical treatment of integration step ($x_P - x_A$). For the numerical solution of the algebraic system at axial station x_P, the integration step size $(x_P - x_A)$ determines the rate at which the longitudinal coordinate x is swept along the duct. In the vicinity of the boundary-layer leading edge ($x \approx 0$), the dependent variable ϕ ($\phi = u, k, \varepsilon,$) varies more rapidly with x, if one considers the initial growth rate of the boundary layer. Therefore, the use of a small but constant value for $(x_P - x_A)$ could be appropriate for the rapid changes of ϕ in the developing region but would imply an excessive number of integration steps at the subsequent developed region. Likewise, a large value for $(x_P - x_A)$ in the beginning of the sweep could, at the inlet region, cause numerical instability due to the large variation of all dependent variables within the initial boundary-layer development.

In this work, the integration step size is adopted as proportional to the distance from the point in question to the beginning of the calculation as

$$\frac{x_P - x_A}{R} = \left(\frac{x - x_I}{x_L - x_1}\right)^{\beta} \tag{15}$$

where indexes I and L correspond to the initial and final x positions, respectively, and R is the duct radius at $x = L$. In Eq. (15) the parameter β gives great flexibility in the choice of the integration step. For $\beta > 1$, the integration step varies more slowly

in the inlet region. Within an area varying duct section, limits I and L in Eq. (15) are reset to diffuser/contraction limits.

Radial distribution of nodal points. In the boundary layer close to the tube wall, the discretization of the production term for k, Eq. (6), is rather sensitive to the radial grid layout. A flexible grid-point distribution is obtained by the use of a coordinate transformation of the type $\phi = r^{\alpha}$, giving for discrete positions along the radial position r,

$$r_i = \left(\frac{R^{\alpha}}{N} - r_{i-1} \right)^{1/\alpha} \tag{16}$$

where i is the index of the nodal point in question and α a parameter for grid control. Note that, for the same number of computational nodes N, an increase of α will concentrate points close to the wall. The location of the first grid point closest to the wall is discussed in some more detail below.

RESULTS AND DISCUSSION

Code Validation

Results for turbulent flow in developing and fully developed tubes were computed with the methodology described herein and were compared with experimental data. This first set of calculations aimed at the validation of the code developed and were presented in detail in [8–10]. Grid independence studies showed that for more than 30 nodal points in the radial direction, the solution is nearly grid-independent. An illustration is presented in Figure 2. Nondimensional velocity distribution u/U_m along the axial coordinate x/D for several radial positions was extensively analyzed in [10] and [23]. Results therein were compared with experimental data of Barbin and Jones [24] for $\mathrm{Re} = 388{,}000$. Computations by Braga [23] for the fully developed region were also extensively compared with the classical experiments of Laufer [25]. Ultimately, extensive validation of the code was accomplished and reported in a number of previous articles. That previous work assured the correctness of the code used in the computations herein.

Proposed Correlation for the Nodal Point Closest to the Wall

Several correlations for the Darcy (Moody) friction factor f defined by

$$f = \frac{8\tau_w}{\rho U_m^2} \tag{17}$$

are compiled in Table 1. Those correlations are valid for a smooth tube and are presented in Kakaç [29], Table 2 shows values for computed f compared with same factors calculated with the correlations of Table 1, but for different radial positions y_N^+ [see Eq. (12)] for the grid point closest to the wall (Figure 1*b*). Noted is the general agreement of the calculated values with those from the literature. Also observed is

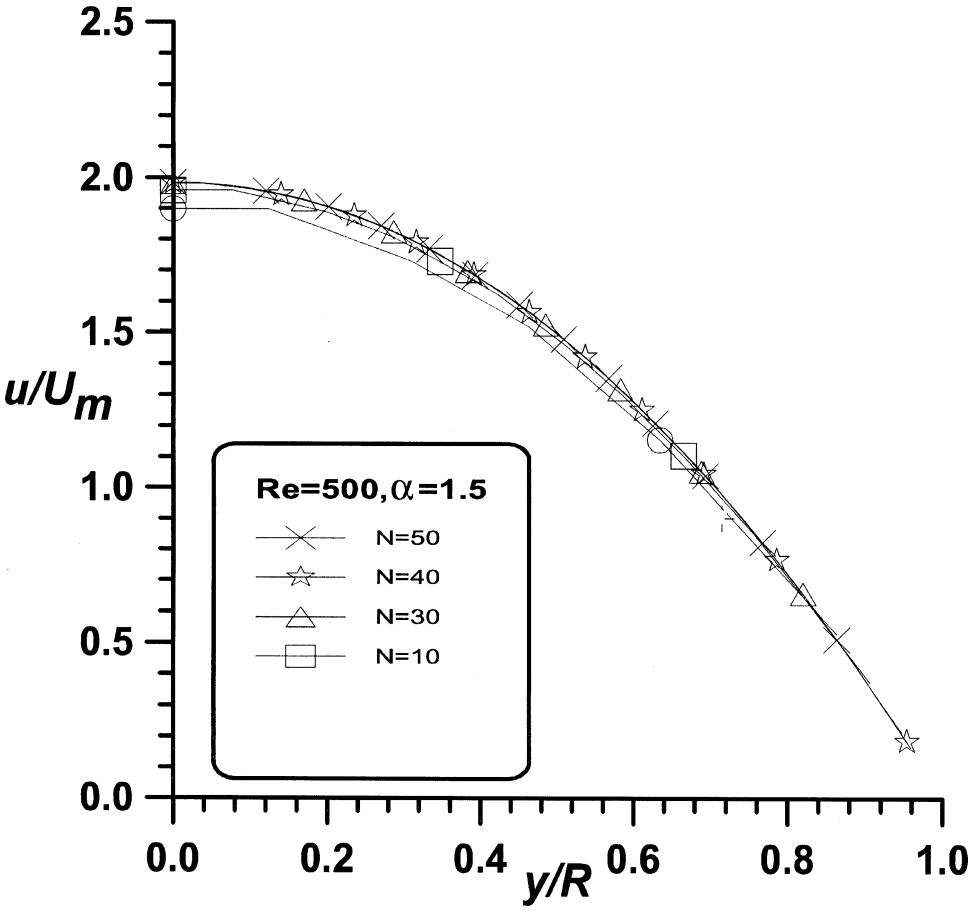

Figure 2. Effect of number of nodal points N on u/U_m, $\mathrm{Re} = 500$.

the existence of an optimal value for y_N^+ for a certain Re. According to Matsumoto and de Lemos [8], the dependence of this optimal value for y_N^+ on Re was considered in the proposed correlation for circular tubes,

$$y_N^+|_{\text{optimal}} = 6,2849 \times 10^{-4}\,\mathrm{Re} + 6.1452 \tag{18}$$

The main idea of Eq. (18) is to use an optimal grid layout depending on the range of Re of the flow. Table 3 presents results for the friction factor for several Re

Table 1. Correlations for turbulent flow in smooth pipe by Kakaç [29]

Reference	Correlation
Blasius	$f_B = 4(0.0791\ \mathrm{Re}^{-0.25})$
Drew, Koo, & McAdams	$f_D = 4(0.00140 + 0.125\ \mathrm{Re}^{-0.32})$
von Kármán & Nikuradse	$f_{KN} = 4[(3.64 \log \mathrm{Re} - 3.28)^{-2}]$
Flonenko	$f_F = 4/(1.58 \ln \mathrm{Re} - 3.28)^2$
Techo, Tickner, & James	$f_T = 4\left[1.7372 \ln\left(\frac{\mathrm{Re}}{1.964 \ln \mathrm{Re} - 3.8215}\right)\right]^{-2}$

Table 2. Calculated f values with correlations of Table 1 (Re = 388,000)

y_N^+	f_{calc}	f_{calc}/f_B	f_{calc}/f_T	f_{calc}/f_D	f_{calc}/f_{KN}	f_{calc}/f_F
100	0.01398	1.10427	1.01356	1.01747	1.01747	1.01628
175	0.01387	1.09549	1.00558	1.00946	1.00946	1.00829
200	0.01384	1.09312	1.00341	1.00728	1.00728	1.00611
225	0.01382	1.09154	1.00196	1.00582	1.00582	1.00465
250	0.01380	1.08996	1.00051	1.00437	1.00437	1.00320
275	0.01378	1.08838	0.99906	1.00291	1.00291	1.00175
300	0.01376	1.08680	0.99761	1.00146	1.00146	1.00029
325	0.01375	1.08601	0.99688	1.00073	1.00073	0.99956
400	0.01369	1.08113	0.99253	0.99636	0.99636	0.99520

Table 3. Influence of Re on f with optimal y_N^+

Re	y_N^+	f_{calc}	f_B	f_T	f_D	f_{KN}	f_F	e_B (%)	e_T (%)	e_D (%)	e_N (%)	e_F (%)
50,000	38	0.02096	0.02113	0.02091	0.02128	0.02093	0.02096	0.80	0.24	1.50	0.14	0.00
388,000	250	0.01380	0.01266	0.01379	0.01374	0.01374	0.01376	9.00	0.07	0.44	0.44	0.29
500,000	320	0.01327	0.01188	0.01316	0.01310	0.01311	0.01313	11.70	1.14	1.30	1.22	1.07

values calculated with optimum values for y_N^+ from Eq. (18). Also presented are the relative errors when the same friction factor is calculated with the correlations of Table 1. The relative error is calculated as

$$e_{correl} = \frac{f_{calc} - f_{correl}}{f_{correl}} \times 100 \tag{19}$$

where correl = B, D, KN, F, or T, depending on the reference cited. Independent of the correlation used (except Blasius, valid up to Re = 10,000), the results show reasonable agreement with the literature cited.

Duct of Varying Cross Section

This section presents results for two flow cases considering converging and diverging sections. Simulations are presented for the hydrodynamic field, mean velocity and turbulent kinetic energy being presented. Herein, the main features of the flow past a conical diffuser or contraction are calculated. For both air and water, profiles of u/U_m and $k/U_m{}^2$ were compared against experimental values and numerical calculations. As mentioned, the results that follow were compared with measurements of Spencer et al. [1], who reported data for air and water in contracting and expanding ducts. In that work, a compilation of the combined effort by 11 European institutions in measuring and simulating turbulent flow past conical diffusers and enlargements was reported. A schematic of the test rigs used is reproduced in Figure 3, containing also all dimensions used to simulate the experiments reported by Spencer et al. [1]. Measurements were reported for air and water in addition to calculations obtained with commercial CFD codes.

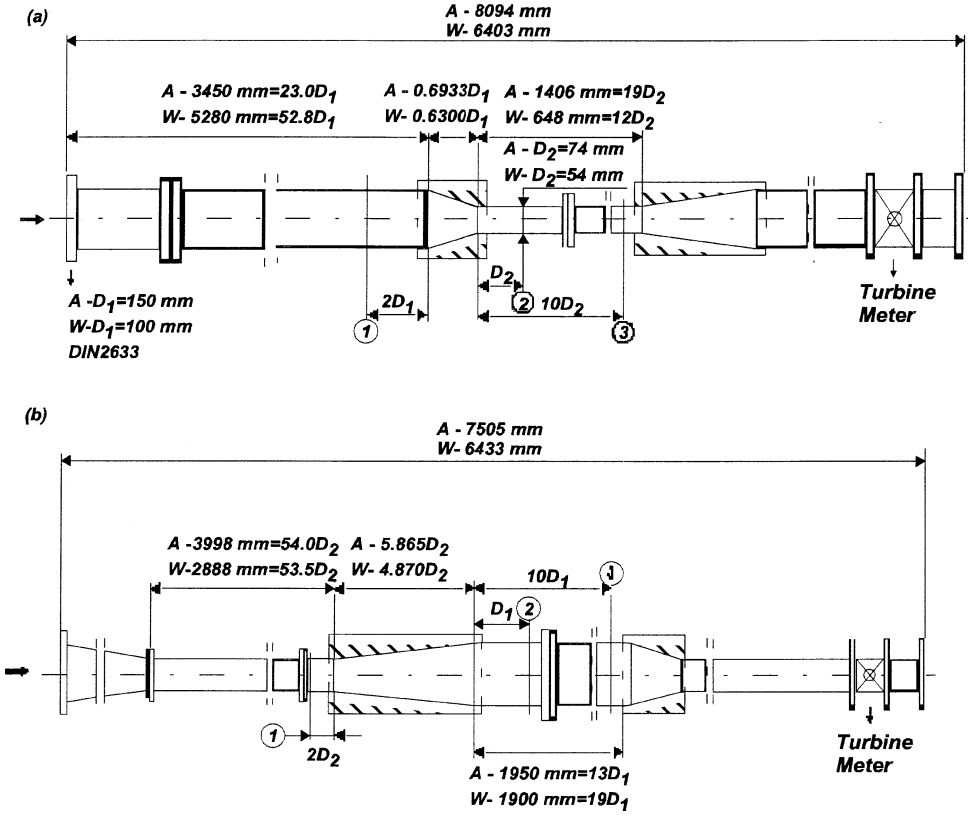

Figure 3. Experimental setup used by Spencer et al. [1].

Contraction. Figure 4 show results for mean velocity at stations 1, 2, 3 of a contraction (Figure 3, upper drawing). Due to symmetry in $y=0$, present simulations cover the range $0<y/R<1$ only (thick lines). To emphasize the spread in the results reported by Spencer et al. [1], the experiments therein were combined into three groups, Lab-A, Lab-B and Lab-C. Numerical runs, also reported by Spencer et al. [1], were also recast into the groups Calc-1, related to the use of the k–ε model, and Calc-2, where an algebraic stress model (ASM) for turbulence was used. These so-called groups of results, either experimental or numerical, express the proximity of different data sources when compared against each other. The existence of different groups of results is a clear indication that even for simple engineering flows, measuring and calculations can differ quite a bit if taken at different places, using different techniques and equipment.

Also, although not stated explicitly in the text, the use of commercial codes in Spencer et al. [1] is an indication of solution being sought with elliptic solvers rather than with the simpler parabolic approach as adopted here. It is equally important to note that all calculations reported by Spencer et al. had as inlet boundary condition the experiments in station 1, always before the area-change section, either for contractions or diffusers, for both air and water runs. Therefore, computation presented

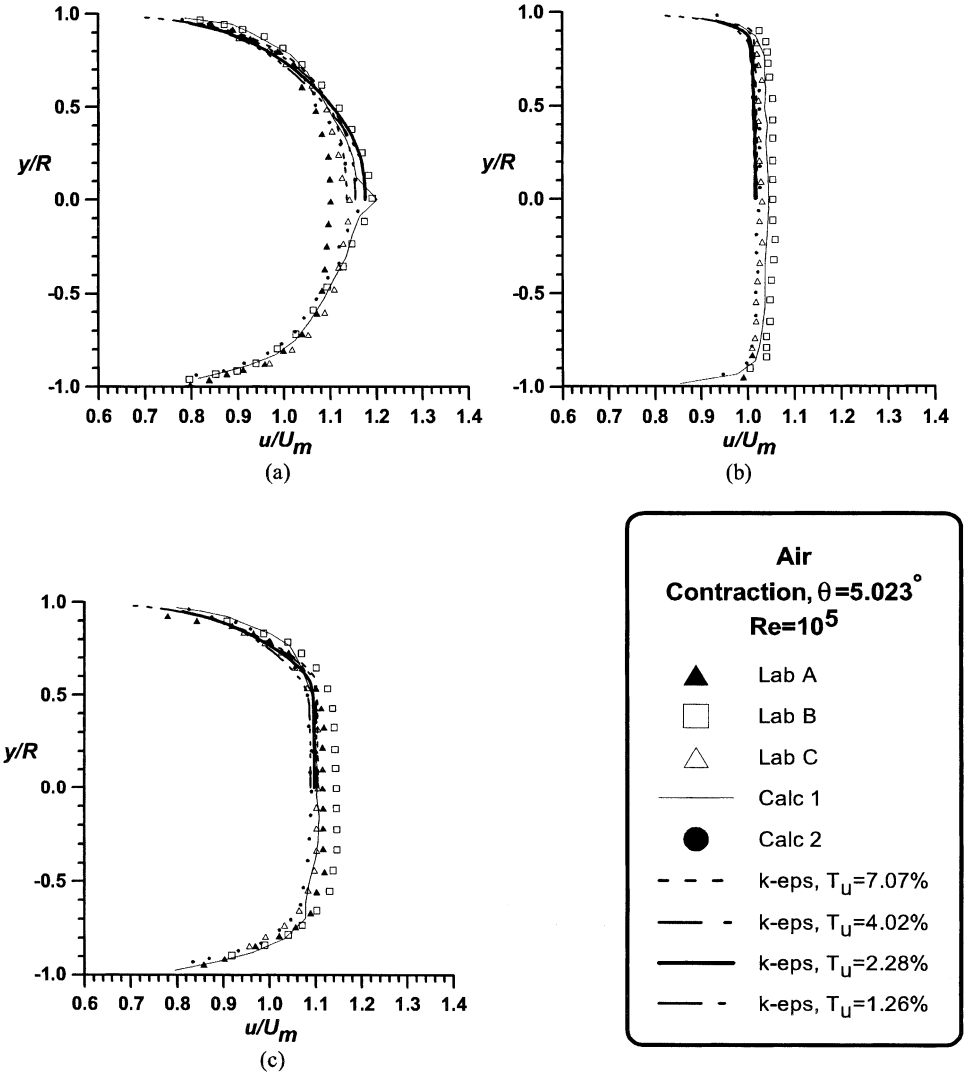

Figure 4. Nondimensional velocity profiles for air flow in a contraction (see Figure 3 for station location): (*a*) station 1 ($x/D=21$); (*b*) station 2 ($x/D=24.1933$); (*c*) station 3 ($x/D=28.6933$).

by Spencer et al. are expected to agree at all stations 1, as they do in Figure 4*a*. On the other hand, the present calculations had an inlet developing region simulated first, beginning at several diameters upstream of station 1. In addition, boundary conditions applied here, instead of using measured values at section 1 of test rigs, were always given as flat profiles for u and by Eqs. (7) and (8) for k and ε, respectively, not at station 1, but rather at the beginning of the just-mentioned inlet length. This procedure was adopted such that at station 1 we had enough boundary-layer growth so that calculations would match the reported experimental profiles. The agreement with experiments and the present simulations at station 1 is then, as expected, clearly seen in all figures.

Corresponding turbulence kinetic energy is presented in Figure 5 for sections 1, 2, and 3. The present results were calculated with different inlet turbulence intensities, giving distinct inlet values for k at the inlet according to Eq. (10). In Figure 5, results are presented for Tu = 1.26, 2.28, 4.02, and 7.07% and show that an effect is obtained at the inlet section 1, particularly at the pipe center, but little influence on the overall k values seems to exist downstream in the flow. The most striking feature to be noted, however, is the perfect follow-up to the problem physics by the present method, showing the damping of turbulence as the flow passes the contraction. This important feature, further discussed in the results show below, could not be correctly reproduced with more sophisticated models (ASM) and numeric tools (elliptic solvers) compared by Spencer et al. [1].

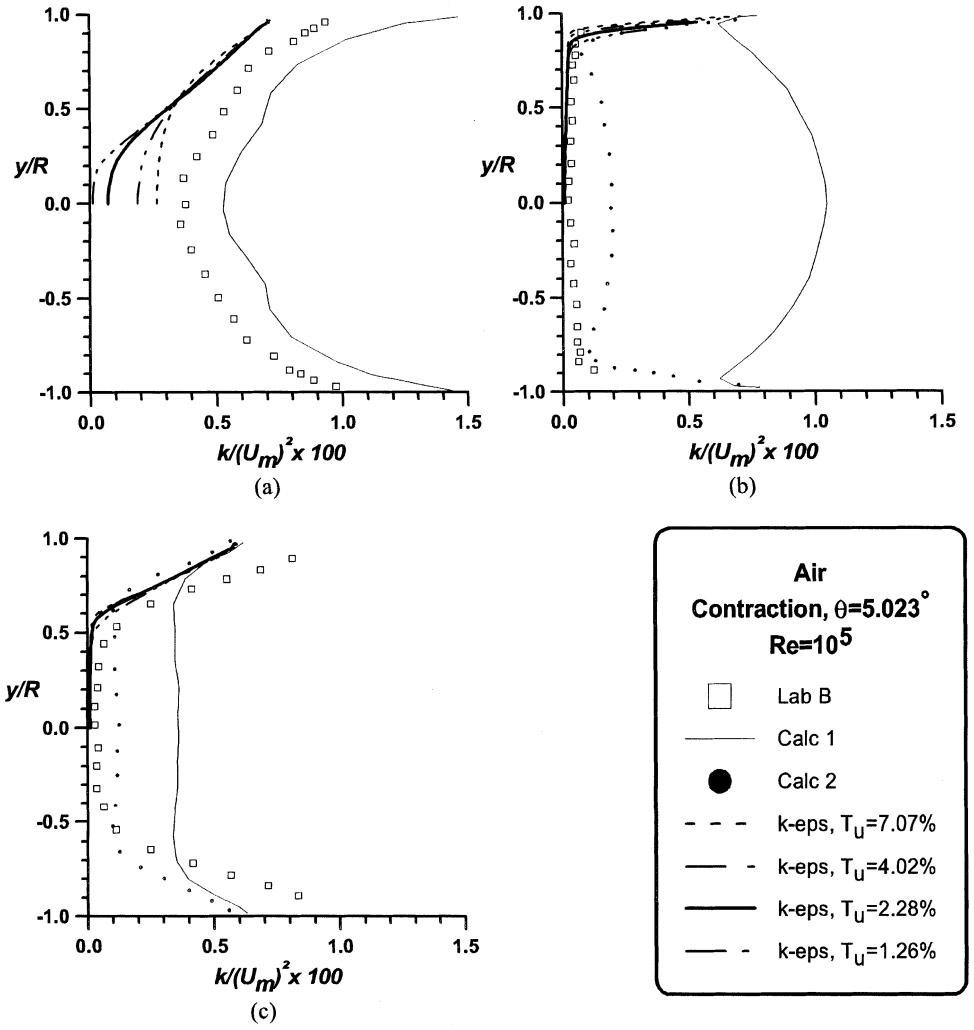

Figure 5. Profiles of k/U_m^2 for air flow in a contraction (see Figure 3 for station location): (*a*) station 1 ($x/D = 21$); (*b*) station 2 ($x/D = 24.1933$); (*c*) station 3 ($x/D = 28.6933$).

Similar results through the contraction of test rig in Figure 3 for water are presented in Figure 6 for u/U_m and Figure 7 for $k/U_m{}^2$. Basically, the same features are also found here, showing the correctness of the methodology employed when compared with experimental evidence.

Diffuser. In a diffuser, the flow is subjected to an adverse pressure gradient. For the conditions of the measurements, separation was indeed observed as pointed out by Spencer et al. [1], for air, although no information on the size of the recirculating region was reported. Here, it is also important to emphasize that, in principle, the overall calculation in diffusers depends much more on the turbulence model than it does on contracting ducts. Enhancement of turbulence makes turbulence terms of a greater importance in the momentum equation (2). Other factors, however, also

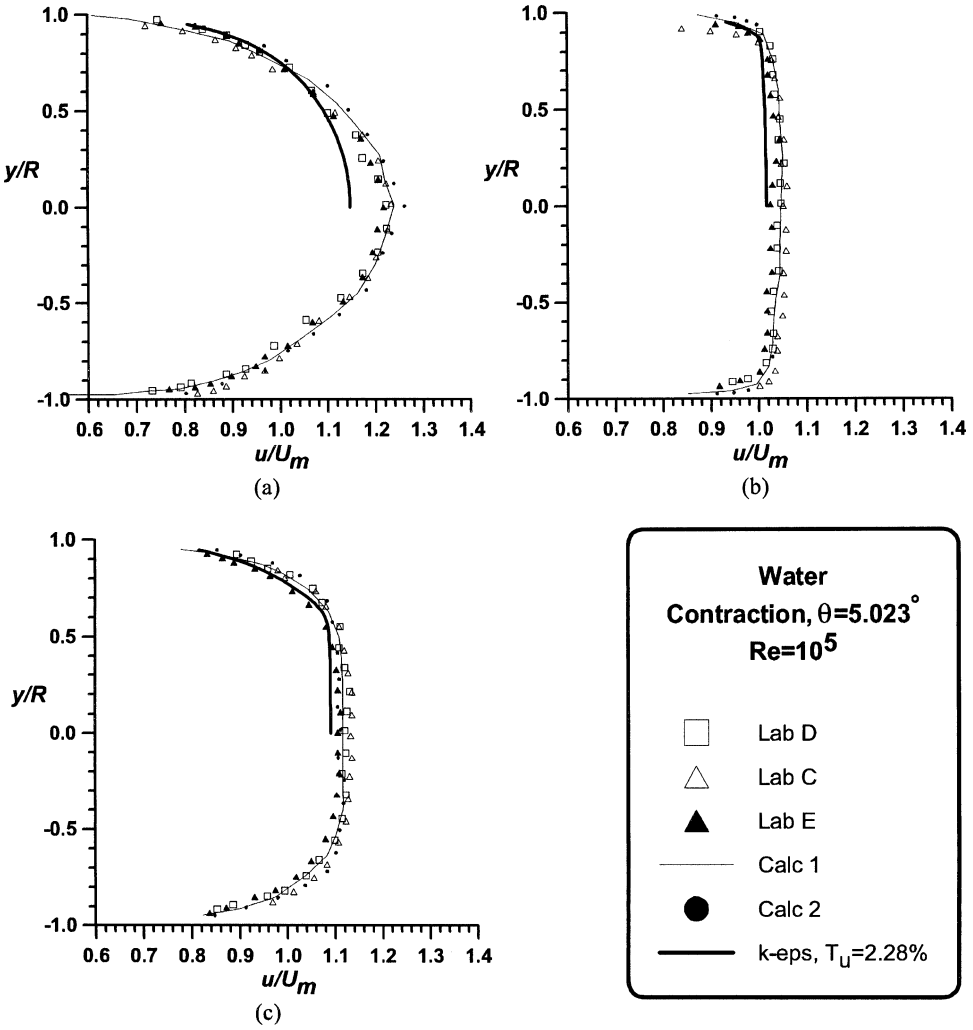

Figure 6. Nondimensional velocity profiles for water flow in a contraction (see Figure 3 for station location): (*a*) station 1 ($x/D = 50.8$); (*b*) station 2 ($x/D = 53.93$); (*c*) station 3 ($x/D = 58.43$).

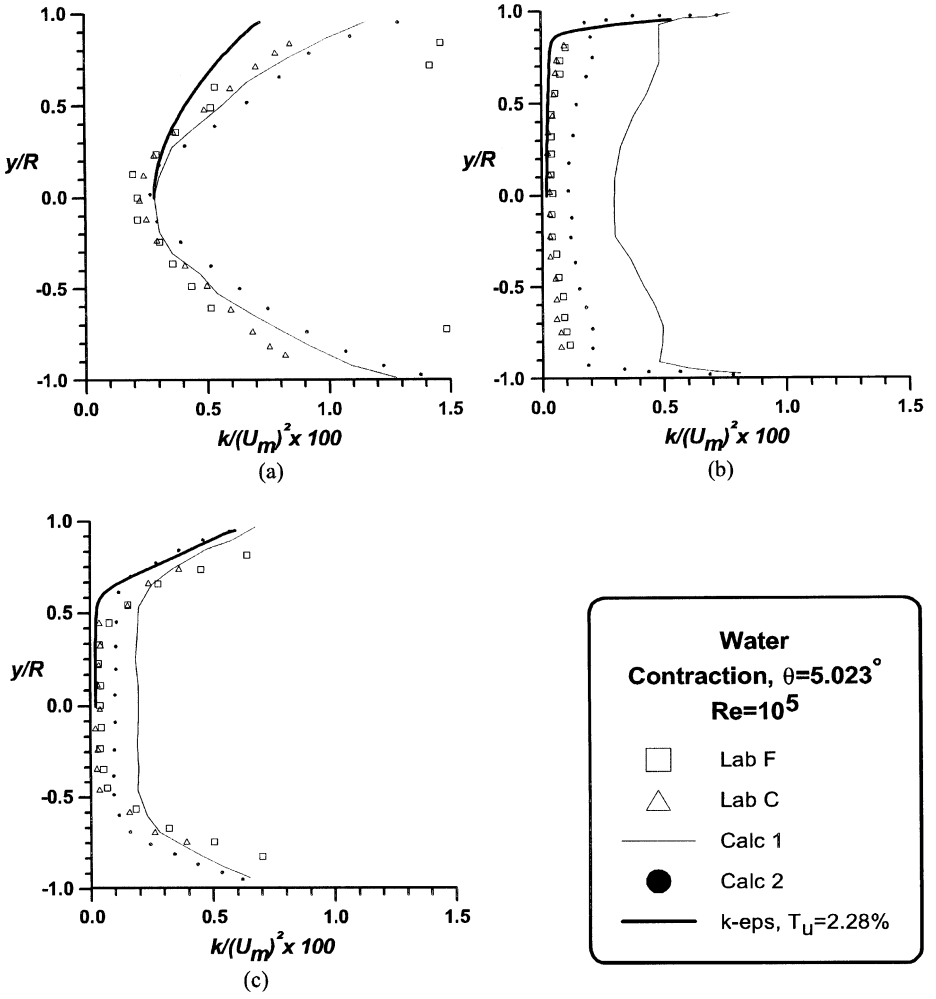

Figure 7. Profiles of k/U_m^2 for water flow in a contraction (see Figure 3 for station location): *a*) station 1 ($x/D = 50.8$); *b*) station 2 ($x/D = 53.93$); *c*) station 3 ($x/D = 58.43$).

affect the quality of the predictions. When using parabolic solvers, proper grid layout, appropriate integration step size relative to boundary-layer thickness, number of visited x stations, and care in handling the unknown pressure gradient can substantially improve numerical stability and results accuracy.

Figures 8 and 9 shows comparisons for u/U_m and $k/U_m{}^2$, respectively. The lines represented by Calc in the figures are computations performed with an algebraic stress model rather than the simpler linear k–ε here employed. Profiles calculated at station 1, for u/U_m (Figure 8a) and for $k/U_m{}^2$ (Figure 9*a*), did not quite match those of the other calculations, most likely due to the distinct methodologies as explained earlier. In this work a developing length was calculated first, before the diffuser inlet. Also, turbulence intensities at the beginning of all diffuser calculations were maintained at 2.28%.

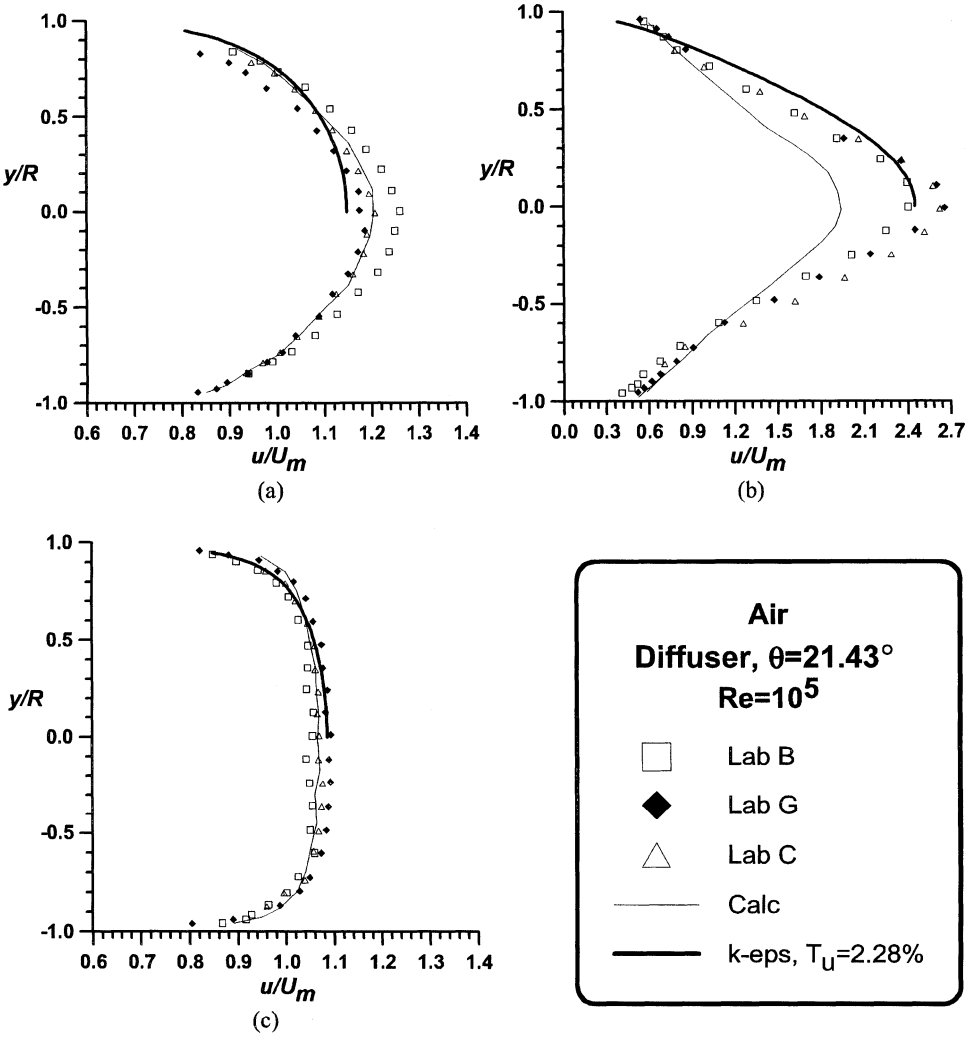

Figure 8. Nondimensional velocity profiles for air flow in a diffuser (see Figure 3 for station location): (*a*) station 1 ($x/D = 52$); (*b*) station 2 ($x/D = 61.865$); (*c*) station 3 ($x/D = 79.865$).

The striking feature of Figures 8 and 9 is that in spite of using a parabolic solver and a linear k–ε model, the present calculations seem to be of comparable quality to those obtained with an ASM model of turbulence. Bulging of the mean velocity profile (Figure 8*b*) is even closer to experiments than the ASM calculations. In measuring section 2, Figure 9*b* also reveals quite a difficulty in recovering the correct levels of k, in either set of calculations. At station 3 (Figure 9*c*), the standard k–ε model also gives closer agreement with experimental data, although values for the turbulent kinetic energy were nearly 30% lower at the wall region.

Similar results for water are presented in Figure 10 for u/U_m and Figure 11 for $k/U_m{}^2$. The general behavior for all curves indicates that the program developed here indeed reproduces the basic features of the flow, namely, the increasing in the

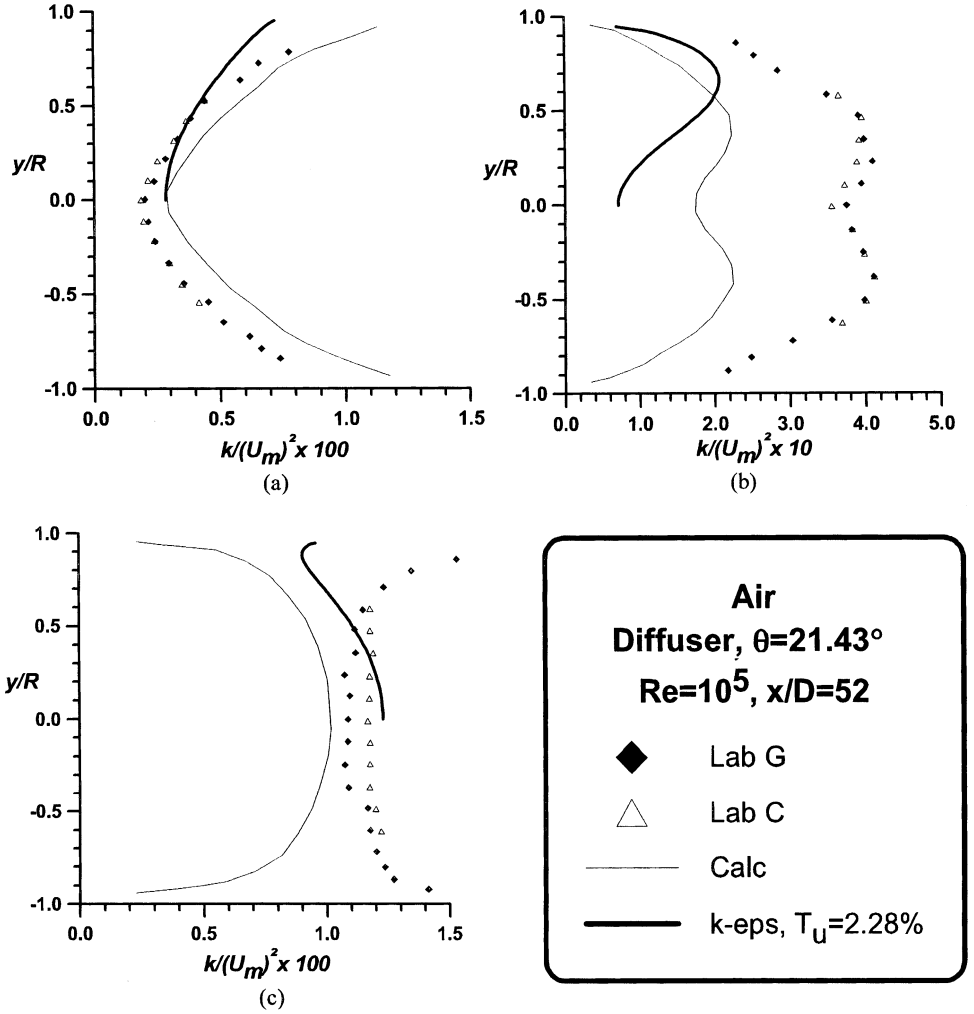

Figure 9. Profiles of k/U^2_m for air flow in a diffuser (see Figure 3 for station location): (*a*) station 1 ($x/D = 52$); (*b*) station 2 ($x/D = 61.865$); (*c*) station 3 ($x/D = 79.865$).

turbulent kinetic energy along expansions and its reduction along contraction, independent of the fluid being used.

In Spencer et al. [1], the overall conclusion was that an advanced turbulence model would do a better job and that "numerical simulation of turbulent flow through simple pipe components cannot be achieved with the commercial programs available." Here, based on the results shown, it is suggested that, for accurate flow prediction, not only the sophistication of the turbulence model matters, but also proper implementation of the numerical model and the use of an adequate tool for the flow in question.

Accordingly, in some practical situations there exists a predominant flow direction, and yet the cross-stream pressure variation is not negligible. Thus, the pressure-decoupling approach employed in the parabolic procedure is not

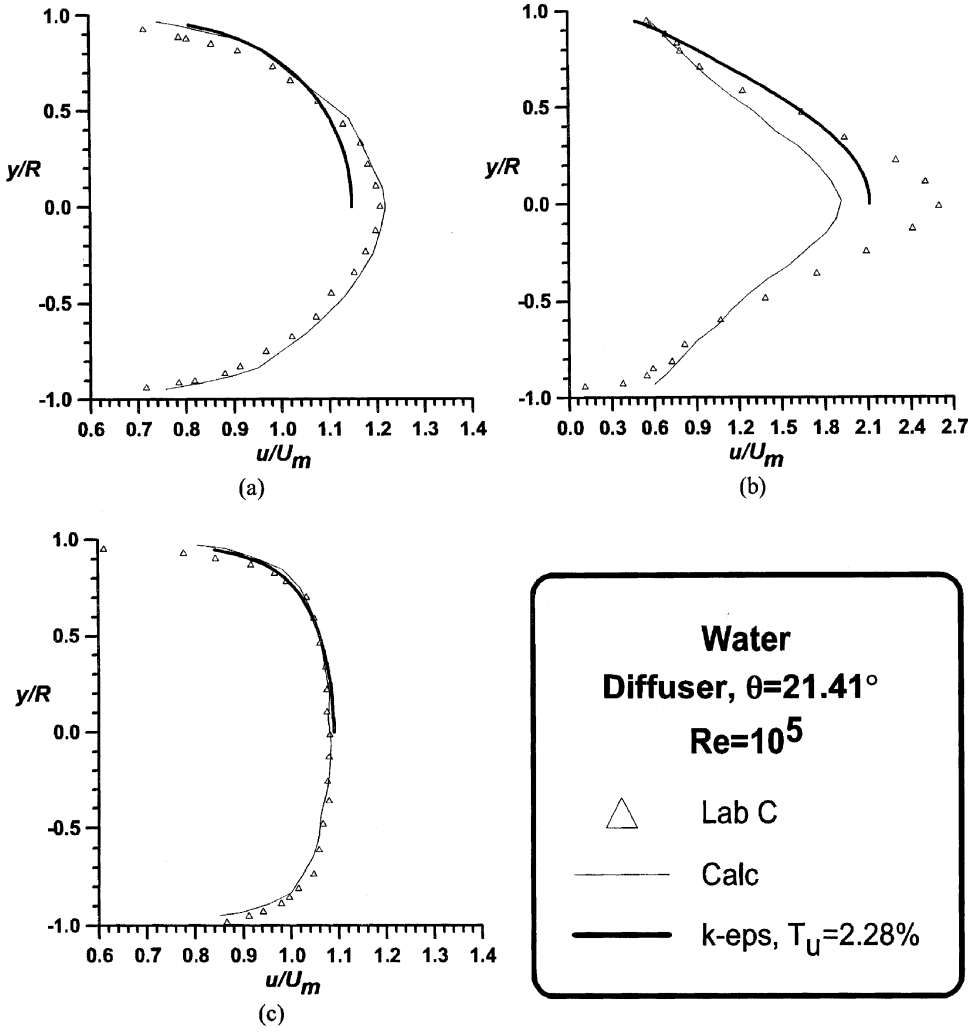

Figure 10. Nondimensional velocity profiles for water flow in a diffuser (see Figure 3 for station location): (*a*) station 1 ($x/D = 51.5$); (*b*) station 2 ($x/D = 60.37$); (*c*) station 3 ($x/D = 78.37$).

appropriate. Except for the pressure, the solution of all other flow variables can be obtained by marching from upstream of the domain to the flow exit. However, important downstream effects transmitted back via pressure cannot be simulated with a parabolic model. Such situations are called partially parabolic flows. Highly curved ducts, jets in cross streams, ducts with a rapid change of cross section, and rotating passages are examples of partially parabolic situations. Pratap and Spalding [26] presented the basic concept of this class of flow.

In the partially parabolic calculation procedure, the pressure field is stored for the entire calculation domain, while all other variables are stored for only one or two marching stations. For a given pressure field, the marching procedure is employed just as in the fully parabolic situation, while an improved pressure field is obtained

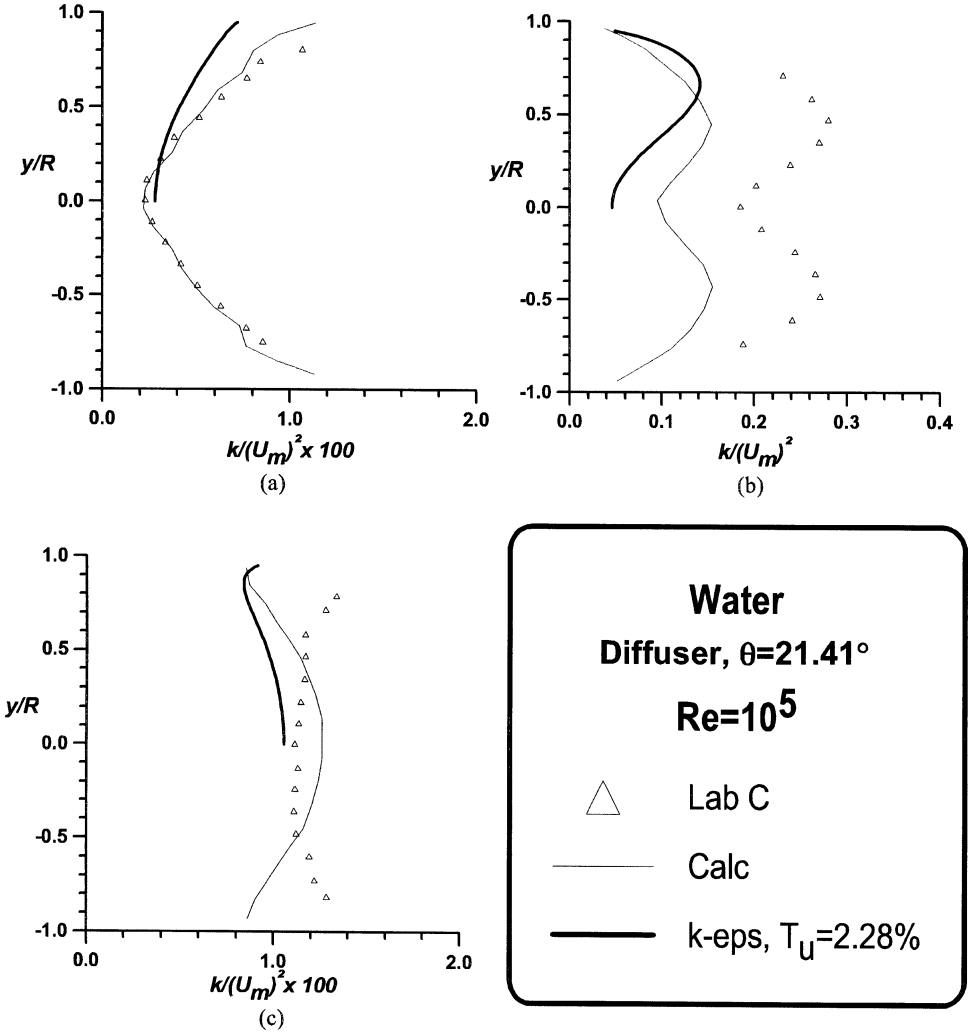

Figure 11. Profiles of k/U^2_m for water flow in a diffuser (see Figure 3 for station location): (*a*) station 1 ($x/D = 51.5$); (*b*) station 2 ($x/D = 60.37$); (*c*) station 3 ($x/D = 78.37$).

from a pressure correction or a pressure equation. Many repetitions of the marching procedure are needed before a converged solution is obtained. Compared with the fully elliptic procedure, the fully parabolic method offers savings in both computer time and storage. The partially parabolic procedure saves storage, but the savings in computer time may not be appreciable [27].

Pressure Coefficient, C_p

Results for the pressure recovery coefficient in diffusers, C_p, defined as

$$C_p = \frac{P_1 - P_2}{\frac{1}{2}\rho u_1^2} \tag{20}$$

are presented in Figures 12*a*, 12*b*, 12*c*, and 12*d* for four values of angle θ. Indexes 1 and 2 in Eq. (20) refer to positions at entrance and exit of the diffuser, respectively (see Figure 1). Results are compared with experiments of Cockrell and Bradley [28]. The length of the conical section of the diffuser is varied for the same angle θ. Pressure recovers as the length of the diffuser increases and flow is decelerated. Further increasing x_c, the velocity close to the walls is reduced, leading eventually to boundary-layer separation. Then, the model presented is no longer valid for rapidly expanding ducts flows. Accordingly, a departure from experimental values can be seen in the figures for lower x_c as the diffuser angle increases. These results are coherent with the idea of limiting the present model to calculation of diffusers with small angles θ. Here, the idea of having engineering estimates of flow in ducts of gradually varying cross section, based on economical parabolic solutions, was the

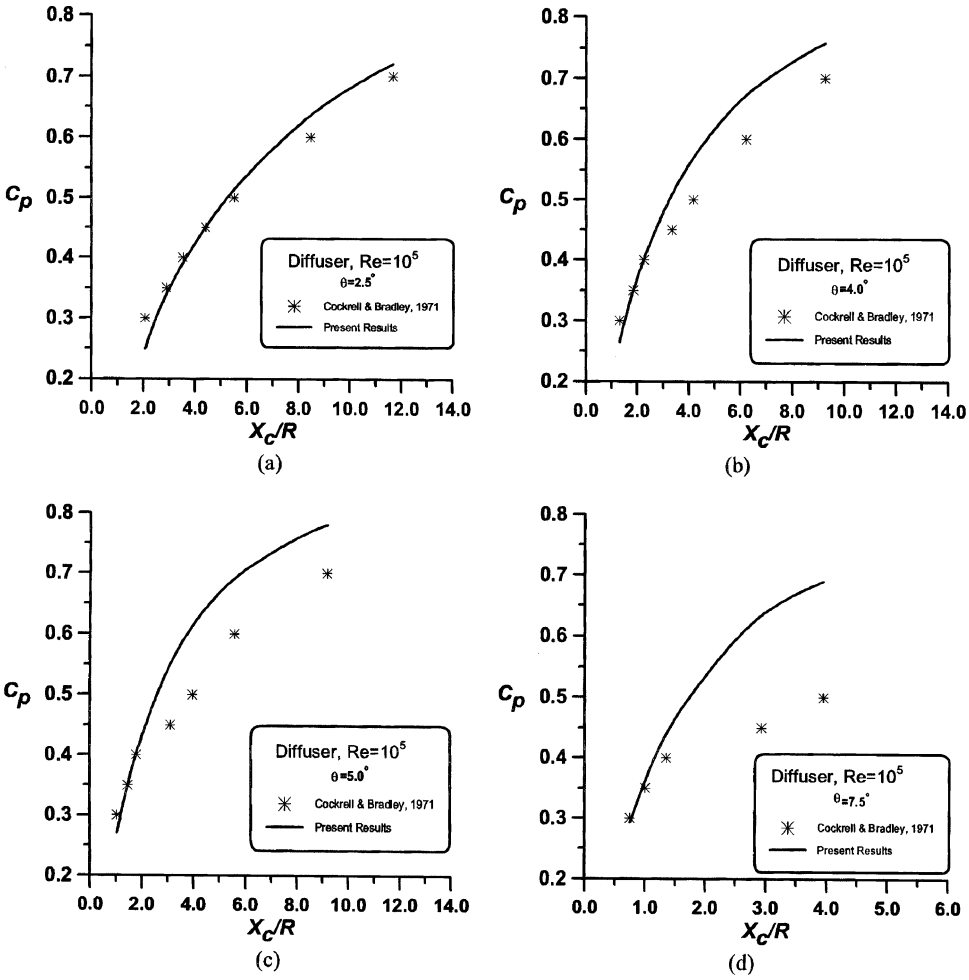

Figure 12. Pressure recovery coefficient for conical diffuser. (*a*) θ = 2.5°; (*b*) θ = 4.0°; (*c*) θ = 5.0°; (*d*) θ = 7.5°.

main motivation of this work. Detailed flow simulation, capturing the elliptic nature of the pressure field and boundary-layer separation, can only be achieved with a proper elliptic formulation.

CONCLUDING REMARKS

This work presented computations with the standard k–ε model for simulation of confined flow in ducts of varying cross section. Diverging and converging ducts were calculated. In general, accelerated flows in a convergent duct reduce turbulence level, and the opposing trend is observed in expanding passages.

Comparisons with classical measurements for fully developed pipe indicate reasonable agreement with the literature. For contractions and diffusers, comparisons with the data bank in Spencer et al. 1995 [1] demonstrated that the methodology employed here, although simple in nature and limited to nonrecirculating flows, gave better or comparable results than those calculated with more sophisticated numerical tools and employing more elaborated turbulence modes. Accuracy of the calculated coefficient of pressure recovery is also limited by the angle and length of the diffuser.

Essentially, this work suggests that, for accurate flow prediction, not only the sophistication of the turbulence model matters, but also proper implementation of the numerical model and the robustness and stability of the algorithm employed. For simple flows, isotropic turbulence theories and simple parabolic codes can provide economical and reliable tools during preliminary steps in the overall design process for engineering equipment.

REFERENCES

1. E. A. Spencer, M. V. Heitor, and I. P. Castro, Intercomparison of Measurements and Computations of Flow Through a Contraction and a Diffuser, *Flow Measure. Instrum.*, vol. 6, no. 1, pp. 3–14, 1995.
2. G. Buresti, P. Petagna, and A. Talamelli, Experimental Investigation on the Turbulent Near-Field of Coaxial Jets, *Exp. Thermal Fluid Sci.*, vol 17, no. 1–2, pp. 18–26, 1998.
3. C. J. Park and L. D. Chen, Experimental Investigation of Confined Turbulent Jets. Part I. Single-Phase Data, *AIAA J.*, vol. 27, no. 11, pp. 1506–1510, 1989.
4. D. Albagli and Y. Levy, Experimental Study on Confined Two-Phase Jets, *J. Thermophys. Heat Transfer*, vol. 5, no. 3, pp. 387–393, 1991.
5. J. Fan, H. Zhao, and K. Cen, Two-Phase Velocity Measurements in Particle-Laden Coaxial Jets, *Chem. Eng. J.*, vol. 63, no. 1, pp. 11–17, 1996.
6. A. Knut and P. Moin, Large-Eddy Simulation of Turbulent Confined Coannular Jets, *J. Fluid Mech.*, vol. 315, pp. 387–411, 1996.
7. A. J. Yule and M. Damou, Axisymmetrical Turbulent Jet Flows in a Duct of Varying Area, *Exp. Thermal Fluid Sci.*, vol. 5, no. 4, pp. 499–505, 1992.
8. E. Matsumoto and M. J. S. de Lemos, Development of an Axi-symmetric Mixing Layer in a Duct of Constant Cross Section, *Proc. 3rd Brazil Thermal. Sciences Meetings*, Itapema, Brazil December 10–12, 1990, vol. I, pp. 381–385.
9. M. J. S. de Lemos and A. Milan, Mixing of Confined Coaxial Turbulent Jets in Ducts of Varying Cross Section, *Proc. COBEM97—12th. Brazil Congress of Mechanical Engineers* (on CD-ROM), Bauru, São Paulo, Brazil, December 8–12, 1997.

10. M. J. S. de Lemos and E. J. Braga, Numerical Investigation of Turbulent Duct Flow through Gradual Enlargements and Contractions, *Proc. FEDSM—Fluid Engineering Division Summer Meeting* (on CD-ROM), Washington, DC, June 21–25, 1998.
11. E. J. Braga and M. J. S. de Lemos, Numerical Analysis of Coaxial Turbulent Jets in Diffusers and Contractions, *Proc. COBEM99—15th Brazil Congress Mechanical Engineers* (on CD-ROM), Águas de Lindóia, SP, Brazil, November 22–26, 1999.
12. M. J. S. de Lemos and E. J. Braga, Simulation of Turbulent Flow in Contracting and Expanding Ducts with a Linear k–ε Model, Paper FEDSM2000–11083, *Proc. 2000 ASME Fluids Engineering Summer Conf.*, Boston, June 11–15, 2000.
13. M. J. S. de Lemos and E. J. Braga, Turbulent Heat Transfer in Confined Coaxial Jets through Ducts of Gradually Varying Cross Section, Turbulent Heat Transfer, Paper NHTC2000–12089, *34th Natl. Heat Transfer Conf.*, Pittsburgh, PA, August 20–22, 2000.
14. W. P. Jones and B. E. Launder, The Prediction of Laminarization with a Two-Equation Model of Turbulence, *Int. J. Heat Mass Transfer*, vol. 15, pp. 301–314, 1972.
15. C. G. Speziale, On Nonlinear k–l and k–ε Models of Turbulence, *J. Fluid Mech.*, vol. 176, pp. 459–475, 1987.
16. W. Rodi, The Prediction of Free Turbulent Boundary Layers by Use of a Two-Equation Model of Turbulence, Ph.D. thesis, University of London.
17. M. J. S. de Lemos and A. Sesonske, Turbulence Modeling in Combined Convection in Liquid-Metal Pipe Flow, *Int. J. Heat Mass Transfer*, vol. 28, no. 6, pp. 1067–1088, 1985.
18. M. J. S. de Lemos, Anisotropic Turbulent Transport Modeling for Rod-Bundle, *Int. J. Heat Technol.*, vol. 6, no. 1–2, pp. 27–37, 1988.
19. B. E. Launder and D. B. Spalding, The Numerical Computation of Turbulent Flows, *Comput. Math. Appl. Mech. Eng.*, vol. 3, pp. 269–289, 1974.
20. S. V. Patankar and D. B. Spalding, A Calculation Procedure for Heat, Mass and Momentum Transfer in Three-Dimensional Parabolic Flows, *Int. J. Heat Mass Transfer.*, vol. 15, pp. 1787–1806, 1972.
21. S. V. Patankar, Parabolic Systems, in W. J. Minkowycz, E. M. Sparrow. G. E. Scheider, and R. H. Pletcher (eds.) *Handbook of Numerical Heat Transfer*, Wiley, New York, 1988.
22. B. E. Launder and D. B. Spalding, Lectures in Mathematical Models of Turbulence, Academic Press, New York, 1972.
23. E. J. Braga, Turbulent Heat Transfer and Fluid Flow in Ducts of Gradually Varying Cross Section, M.Sc. thesis, ITA, São José dos Campos, SP, Brazil, 1999.
24. A. R. Barbin and J. B. Jones, Turbulent Flow in the Inlet Region of a Smooth Pipe, *J. Basic Eng.*, vol. 85, no. 1, pp. 29–34, 1963.
25. J. Laufer, The Structure of Turbulence in Fully Developed Pipe Flow, NACA-TR-1174, 1954.
26. V. S. Pratap and D. B. Spalding, Numerical Computation of the Flow in Curved Ducts, *Aeronaut. Q.*, vol. 26, p. 219, 1975.
27. S. V. Patankar, *Numerical Heat Transfer and Fluid Flow*, McGraw-Hill, New York, 1980.
28. D. J. Cockrell and C. L. Bradley, The Response of Diffusers to Flow Conditions at Their Inlet, Paper 5, *Symp. on Internal Flows*, University of Salford, UK, 1971, pp. A32–A41.
29. S. Kakaç, Boilers, Evaporators and Condensers, p. 90, Wiley, New York, 1991.